JACS
JOURNAL OF THE AMERICAN CHEMICAL SOCIETY

Article

pubs.acs.org/JACS

Fluorescence Discrimination of Cancer from Inflammation by Molecular Response to COX-2 Enzymes

Hua Zhang,[†] Jiangli Fan,*[,†] Jingyun Wang,[‡] Bairui Dou,[‡] Fan Zhou,[⊥] Jianfang Cao,[†] Junle Qu,[⊥] Zhi Cao,[§] Weijie Zhao,[§] and Xiaojun Peng*[,†]

[†]State Key Laboratory of Fine Chemicals, [‡]School of Life Science and Biotechnology, and [§]School of Pharmaceutical Science and Technology, Dalian University of Technology, 2 Linggong Road, Hi-tech Zone, Dalian 116024, People's Republic of China

[⊥]Key Laboratories of Optoelectronic Devices and Systems of Ministry of Education, Shenzhen University, Shenzhen 518060, People's Republic of China

Supporting Information

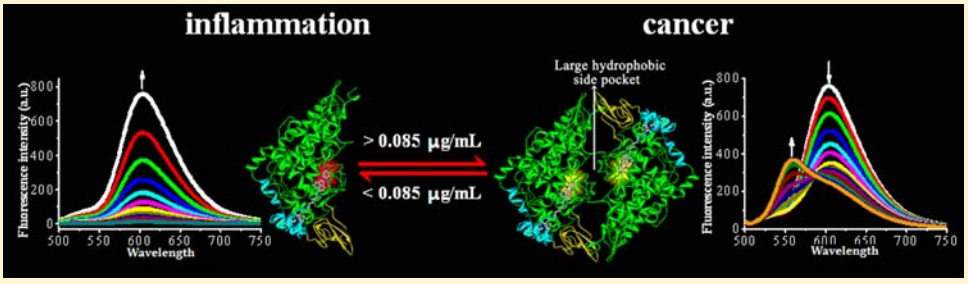

ABSTRACT: Accurate identification of cancer from inflammation and normal tissue in a rapid, sensitive, and quantitative fashion is important for cancer diagnosis and resection during surgery. Here we report the use of cyclooxygenase-2 as a marker for identification of cancer from inflammation and the design of a novel smart COX-2-specific fluorogenic probe (NANQ-IMC6). The probe's fluorescence is "turned on" in both inflammations and cancers where COX-2 is overexpressed. Intriguingly, the fluorescent emission is quite different at these two sites with different expression level of COX-2. Hence, NANQ-IMC6 can not only distinguish normal cells/tissues from cancer cells/tissues but also distinguish the latter from sites of inflammation lesions by the different fluorescence recognition of NANQ-IMC6 for COX-2 enzymes. Following spraying with the NANQ-IMC6 solution, cancerous tissue, inflamed tissues, and normal tissues can be accurately discriminated in vivo by the unaided eye using a hand-held ultraviolet lamp emitting at 365 nm. So the probe may have potential application varying from cancer inflammation diagnosis to guiding tumor resection during surgery.

INTRODUCTION

Cancer is a major disease worldwide, currently resulting in the deaths of over 7 million people annually, and is predicted to become an even greater problem over the next 20 years.[1] One factor markedly influencing cancer mortality is the difficulty of obtaining accurate early diagnoses, when tumors are more treatable. For example, cancers are sometimes misdiagnosed as inflammations since the symptoms of cancers in the early stage are similar with that of inflammation.[1] At present, standard diagnostic methods of cancer detection—such as cyto- or histopathological examination of biopsies and nuclear magnetic resonance—are often not effective until the middle to late stages of disease, which results in delayed diagnosis, often after metastasis and diffusion have occurred.[2−5] Furthermore, tumor persistence or recurrence, due to incomplete resection during surgery, is another challenge for cancer treatment. Consequently, there are strong motives to seek improved procedures both for early and accurate diagnosis and for the visualization of localized and disseminated cancerous tissues from inflammation in patients—ideally using the same methodology.

Fluorescence imaging methods, using active probes, offer a promising strategy for the selective visualization of malignant tumors because of the high-selectivity, high-resolution, non-invasive real-time capabilities of such reagents. Moreover, these probes avoid the radiological hazards resulting from current imaging technologies such as positron emission tomography, single-photon emission computed tomography method, and X-ray imaging.[1−6] With this in mind, Urano and colleagues[2] recently reported an activated fluorescent probe, gGlu-HMRG, which targeted γ-glutamyltranspeptidase (GGT), an enzyme overexpressed on the surface of some cancer cells including hepatic cancer and glioma.[6−8] More appropriate protein imaging target overexpressed in different cancers would therefore be discovered and studied.

Cyclooxygenase-2 (COX-2) is a promising candidate of cancer imaging target, as it is highly expressed in tumors, such as stomach cancer, pancreas cancer, colon cancer, and so on. As an inducible enzyme used for imaging in clinical medicine,[9−12]

Received: August 17, 2013
Published: October 22, 2013

dx.doi.org/10.1021/ja4085308 | J. Am. Chem. Soc. 2013, 135, 17469−17475

COX-2 expresses at different levels in inflammatory lesions and in tumors, but barely in the normal cells.[13−17] The clinical data suggest that overexpression of COX-2 is associated with all stages of cancers, from the earliest premalignancy phase to metastasis and diffusion.[18−20] Moreover, the amount of COX-2 increases as cancer progresses.[21−23] Recently, Marnett et al.[23] reported a promising fluorescence method using COX-2-specific molecular probes. In our previous work, an off-on probe for Golgi of the cancer cell was published based on COX-2 as the imaging target.[24] Unfortunately, these reports fail to discriminate tumors from inflammation, a considerable clinical limitation.

Here we report a novel smart COX-2-specific fluorogenic probe, NANQ-IMC6, which can not only distinguish normal cells/tissues from cancer cells/tissues but also cleverly distinguish the latter from sites of inflammation. NANQ-IMC6 is nonfluorescent in the absence of COX-2. The probe's fluorescence is "turned on" in both inflammatory lesions and tumors where COX-2 is overexpressed. To our excitement, the fluorescent emission is quite different at these two sites. The probe design is based on linking a chemically modified indomethacin (IMC), a substrate of COX-2, to a nitro-acenaphthenequinone (NANQ) fluorophore, via a carbon linker that fits in the flexible COX-2 substrate-specificity loop. In silico structural analyses and the outcome of whole-cell assays demonstrated the rapid and quantitative response of NANQ-IMC6 to COX-2 with high selectivity and sensitivity. Cancers could be distinguished from inflammations based on labeling with NANQ-IMC6.

RESULTS AND DISCUSSION

Design Strategy of COX-2-Specific Fluorogenic Probe. COX-2 is not present in most normal tissues and normal cells, and the enzyme is present in inflammatory lesions and expresses at low levels (<0.085 μg/mL) as a monomer (Figure 1a),[25−27] which was verified by enzyme-linked immunosorbent assay (ELISA) in normal cells (HEK 293 cell 0.00045 μg/mL, COS-7 cell 0.0075 μg/mL), normal tissues (0.0056 μg/mL), and inflammatory tissues (0.064 μg/mL). Each COX-2 monomeric unit is composed of three distinct structural domains: a short N-terminal epidermal growth factor (EGF) domain (brown domain), the α-helical membrane binding domain (the lobby, blue domain), and the C-terminal catalytic domain (green domain).[25−29] However, in tumor cells and tumor tissues, for example, HT-29 (2.46 μg/mL), HeLa (2.13 μg/mL), MCF-7 (3.76 μg/mL), and tumor tissues (4.52 μg/mL), COX-2 expresses at high levels (>0.085 μg/mL) and exists as a homodimer (Figure 1a). The binding pocket of indomethancin, composed of Arg120, Tyr355, and Glu524 (Figure 1b), is located at the end of a long channel that runs from the wide lobby domain at the protein surface to the narrow interior of the protein.[30,31] A nitro-acenaphthene-quinone dye was selected as the fluorophore for its excellent stability and for the sensitive response of its fluorescence to environmental change. A linear alkyl diamine was chosen as the linker that forms an amide bond with indomethancin at one end and a secondary amine bond with the fluorophore at the other end. We envisioned that such a design would give a molecule of the necessary size and flexibility to permit specific binding with COX-2. Considering the effect of the length of the linker, two probes with six-carbon and two-carbon linkers (respectively, NANQ-IMC6 and NANQ-IMC2, Figure 1c) were synthesized, as outlined in Supporting Information Scheme S1, and unambiguously characterized.

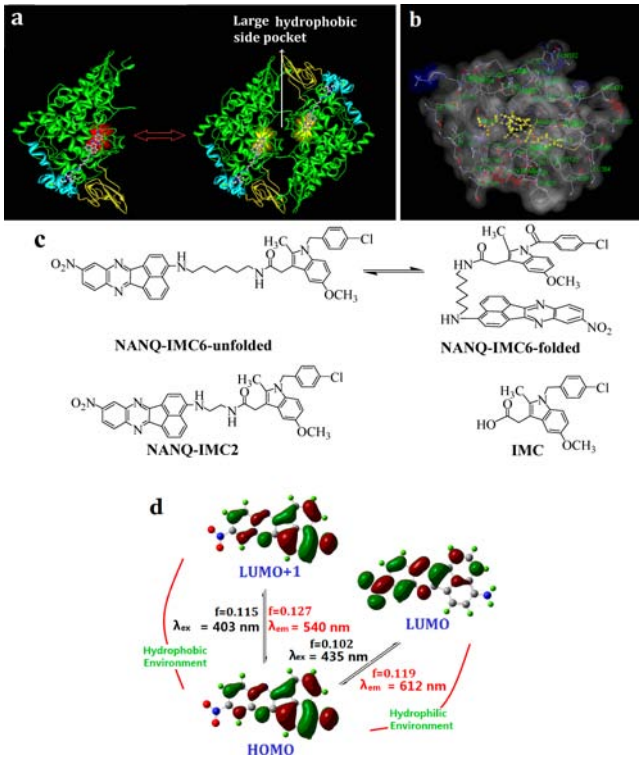

Figure 1. COX-2-specific fluorogenic probe NANQ-IMC6 and its analogue NANQ-IMC2. (a) Crystal structure of cyclooxygenase-2 (COX-2), cited from HPDB. (b) Molecular docking result of NANQ-IMC6. (c) Chemical structures of NANQ-IMC6, NANQ-IMC6-unfolded, NANQ-IMC6-folded, NANQ-IMC2, and IMC. (d) Structural optimization and frontier molecular orbital (MO) of NANQ moieties calculated with time-dependent density functional theory using Gaussian 09. Condition: 100.0 mM Tris-HCl buffer (pH 8.0).

Mechanism of the Fluorescent Response to COX-2. NANQ-IMC6 is nonfluorescent in the absence of COX-2 in Tris-HCl buffer (pH 8.0). After incubation of a low concentration of COX-2 (0.50 μg/mL) with NANQ-IMC6 (5.0 μM), a 55-fold enhancement of fluorescence intensity at 615 nm arose within minutes (Φ_{free} = 0.0034 and $\Phi_{COX\text{-}2}$ = 0.19, Figure 2a). All other biomolecules investigated, including DNA, COX-1, lysozyme, proteinase k, and so on, had no such response (Figure S1).

To elucidate the basis of the fluorescence "off-on" process, the two low-energy conformations of NANQ-IMC6; namely, NANQ-IMC6-unfolded and NANQ-IMC6-folded were optimized using Gaussian 09 (DFT/TDDFT in B3LYP/6-31G level), and their frontier molecular orbital energies in water were calculated. The results showed that the energy of the NANQ-IMC6-folded was 3.3 kcal lower than that of the NANQ-IMC6-unfolded (Figure 1c). This calculation supports the view that unbounded NANQ-IMC6 exists mainly as the folded form (NANQ-IMC6-folded) in the buffer solution. The oscillator strength of NANQ-IMC6-folded in Tris-HCl buffer for the electron transition from HOMO to LUMO is only 0.0027 (Figure S2a), which means that the electron transition from HOMO to LUMO is prohibited. Thus, the fluorescence of NANQ-IMC6-folded is quenched in the absence of COX-2 (Figure 2a). When the indomethacin (IMC) moiety binds to

dx.doi.org/10.1021/ja4085308 | J. Am. Chem. Soc. 2013, 135, 17469−17475

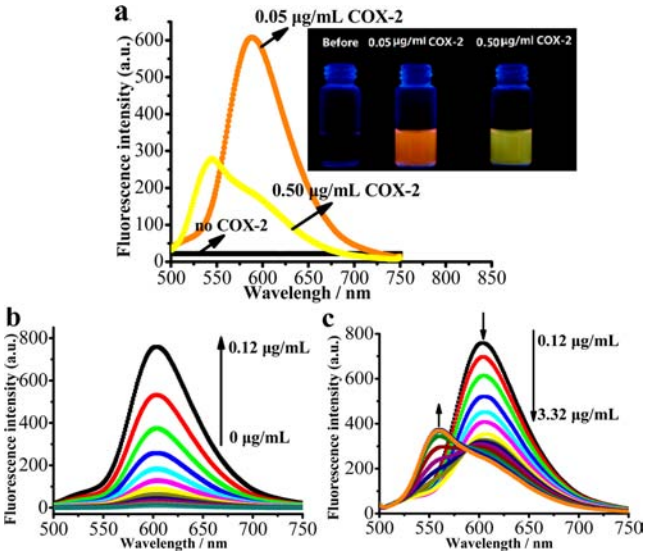

Figure 2. Quantitative detection of COX-2 in vitro. (a) Fluorescence emission spectra of NANQ-IMC6 (3.0 μM) excited at 800 nm in the absence and presence of COX-2 (0.05 and 0.50 μg/mL) in buffer at 25 °C. (b) Fluorescence spectra of NANQ-IMC6 (5.0 μM) in buffer in the presence of COX-2 (0−0.12 μg/mL), excitation wavelength = 463 nm. (c) Fluorescence spectra of NANQ-IMC6 (5.0 μM) in buffer in the presence of COX-2 (0.12−3.32 μg/mL), excitation wavelength = 463 nm. Condition: 100 mM Tris-HCl buffer (pH 8.0).

COX-2, however, the geometry of the binding channel forces the probe to adopt the unfolded conformation, and electron transfer between NANQ and IMC moieties cannot occur, restoring fluorescence (Figure 2a). In the case of NANQ-IMC2, no change was seen in the fluorescence intensity under the same condition (C_{COX-2} = 0.050 μg/mL, Figure S1). This difference between these two probes can be explained by the results of a molecular docking study using Discovery Studio LigandFit software. The linker length of NANQ-IMC2 (6.071−7.071 Å) is shorter than the distance from the binding site to the large hydrophobic channel in COX-2 (8.294−9.294 Å). Thus, NANQ-IMC2 cannot enter the binding pocket and fails to label COX-2 (Figure S2b). The IC_{50} values of NANQ-IMC6, NANQ-IMC2, and IMC for COX-2 were 0.73, 36.78, and 0.75 μM, respectively, indicating that the binding affinity of NANQ-IMC6 for COX-2 was similar to that of IMC and was far stronger than that of NANQ-IMC2.

NANQ-IMC6 showed different fluorescence responses to different concentrations of COX-2 in Tris-HCl buffer solution (pH 8.0, incubation time = 30 min). In low concentrations of COX-2 (<0.12 μg/mL), the fluorescence emission was at 615 nm (Figure 2a,b). There was a linear relationship between fluorescent intensity log (F) and COX-2 concentration over the range 0.0−0.12 μg/mL (Figure S3a and eq S1). However, when the concentration of COX-2 exceeded 0.12 μg/mL, the fluorescence emission at 615 nm decreased gradually, and a new emission at 555 nm showed up and increased with the increasing COX-2 concentration (Figure 2a,c). Consequently, there is a linear fluorescent ratio (I_{555}/I_{615}) response (from 0 to 8.64) to high concentration of COX-2 in the range of 0.12−3.32 μg/mL (Figure S3b and eq S2).

In Figure 1a, we explained the result is from different environments of the unfolded NANQ moiety: hydrophilic environment in low concentration of COX-2 (monomer) and hydrophobic environment in high concentration of COX-2 (homodimer). To determine the reason why the NANQ moiety showed different fluorescence responses to hydrophilic and hydrophobic environments, we calculated the frontier molecular orbital (MO) of NANQ moieties by DFT/T DDFT at the B3LYP/6-31G** level of Gaussian 09. As shown in Figure 1d, from HOMO to LUMO in hydrophilic environment, the electron density transferred from the amino part to the nitro part, which means the nitro group has strong electron-withdrawing effect and increases the intramolecular push−pull electron system. While in the hydrophobic environment, the electron density does not have such change from HOMO to LUMO+1. The two different excited states produce two different emissions at 612 nm in the hydrophilic environment (water) and 540 nm in the hydrophobic environment (dichloromethane) of NANQ, respectively. The experimental detection of NANQ wavelengths (Figure S3c) was at 595 nm in the hydrophilic environment (water) and 526 nm in the hydrophobic environment (dichloromethane), consistent with the calculation.

In inflammatory lesions, COX-2 expresses at low level (<0.085 μg/mL) as a monomer (Figure 1a).[25−27] When the IMC moiety of NANQ-IMC6 bond to the binding pocket of COX-2, the fluorogenic NANQ moiety was extruded from the protein and thrusted into an aqueous microenvironment, emitting at 615 nm. On the contrast, in tumor tissues such as MKN45, MDA-MB-231, and BEL7402, COX-2 overexpresses at high levels (much greater than 0.085 μg/mL) and exists there as a homodimer (Figure 1a). When the IMC moiety of NANQ-IMC6 bonds to COX-2, the NANQ moiety was included in the large hydrophobic channel of the COX-2 homodimer and emitted at 555 nm. Due to these different emissions, NANQ-IMC6 can thus be used to distinguish cancer tissues both from normal tissues and from inflammatory regions.

Two-Photon Property of NANQ-IMC6. Two-photon microscopy (TPM), which employs two near-infrared photons as the excitation source, offers a number of advantages over single-photon microscopy, including greater penetration depth into tissues, localization of excitation, and longer observation time, due to reduced photobleaching and photodamage. The two-photon emission spectra of NANQ-IMC6 showed a 28-fold enhancement at 555 nm in the presence of COX-2 (0.50 μg/mL) in Tris-HCl buffer at pH 8 compared with that in the absence of COX-2 (Figure S4a). The cross section value ($\Phi\delta_{max}$) of NANQ-IMC6 was as high as 133 GM (1 GM = 10^{-50} cm^4 s/photon) when excited at 800 nm, certainly high enough for TPM.[35] The two-photon excitation process was confirmed by a power dependence experiment (Figure S4b), and is a very important model[32−34] for practical application in quantitative imaging of COX-2 in biosystems.

Quantitative Detection of COX-2 in Live Cancer Cells. After staining with NANQ-IMC6 (5.0 μM, incubation times: 30 min), three cancer cell lines, HT-29, HeLa, and MCF-7, showed rapid and strong fluorescence responses by one- and two-photon-induced fluorescence microscopy. On the contrary, the two normal cell lines, COS-7 and HEK 293, showed no such response (Figure S5). The fluorescence strength was correlated with the concentration of COX-2 present in these cell lines, which was measured by ELISA (Figure S5c).[36] The calculated signal-to-noise ratios were 23- to 55-fold with these cancer cell lines.

Quantitative imaging of COX-2, fluorescence ratio imaging, in live cells can provide very valuable information for accurate

dx.doi.org/10.1021/ja4085308 | J. Am. Chem. Soc. 2013, 135, 17469−17475

diagnosis and treatment of cancer. The active site of COX-2 in cancer cells can be controlled using the high affinity inhibitor celecoxib. When 5.0, 2.5, and 0 μg/mL of celecoxib was delivered into HeLa cells, the intensity of the green channel (555 ± 20 nm) increased (Figure 3a), while the red channel

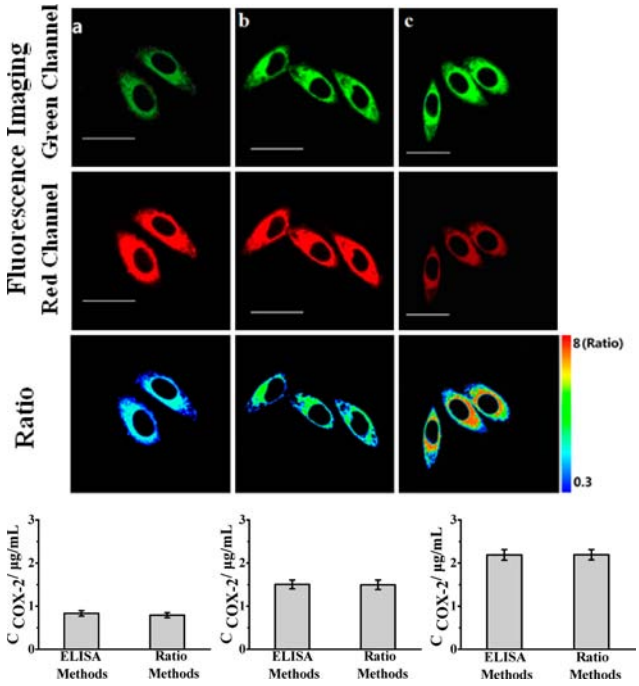

Figure 3. Quantitative detection of COX-2 in live cells by ratio imaging. Celecoxib of 5.0, 2.5, and 0 μg/mL was added in (a–c), respectively. NANQ-IMC6 = 5.0 μM; excitation wavelength = 800 nm; scan range = 555 ± 20 nm (green channel), 615 ± 20 nm (red channel); incubation time = 30 min; scale bars = 30 μm.

(615 ± 20 nm) decreased (Figure 3a). The ratio (F_{555}/F_{615}) images show that the largest increases occurred at the lowest inhibitor levels. The average concentrations of COX-2 estimated by the ratio imaging method were 0.791, 1.505, and 2.192 μg/mL (Figure 3a and eq S2), which were consistent with the ELISA procedure (0.810 ± 0.021, 1.513 ± 0.013, and 2.197 ± 0.012 μg/mL, $P < 0.05$).[11,12,19]

Distinguishing Cancerous and Inflammatory Tissues. To distinguish cancerous tissues from inflammatory tissues, mouse S180 cancerous tissues and inflammatory tissues (5 day and 15 day) were used for NANQ-IMC6 staining experiments. The results from fluorescence ratio imaging (Figure 4a) revealed that the average contents of COX-2 in two cancerous tissues were 0.534 and 5.33 μg/mL, while those in two inflammatory tissues were 0.0347 and 0.0665 μg/mL (Figure 4a and eq S2). These findings were consisitent with the results obtained by the ELISA method (0.527 ± 0.016, 5.21 ± 0.012, 0.0329 ± 0.0015, and 0.0647 ± 0.0017 μg/mL, $P < 0.05$) (Figure 4a).[11,12,19]

Thus cancerous and inflammatory tissues can be distinguished by NANQ-IMC6 by comparing fluorescence images in different channels. The cancerous tissues revealed a strong fluorescence signal in the green channel, while inflammatory tissues showed an image in the red channel, with negligible emission in the green channel (Figure 4b).

Possible Fluorescence-Guided Resection of Tumors. When a Small Animals Living Imaging System (NightOWL II

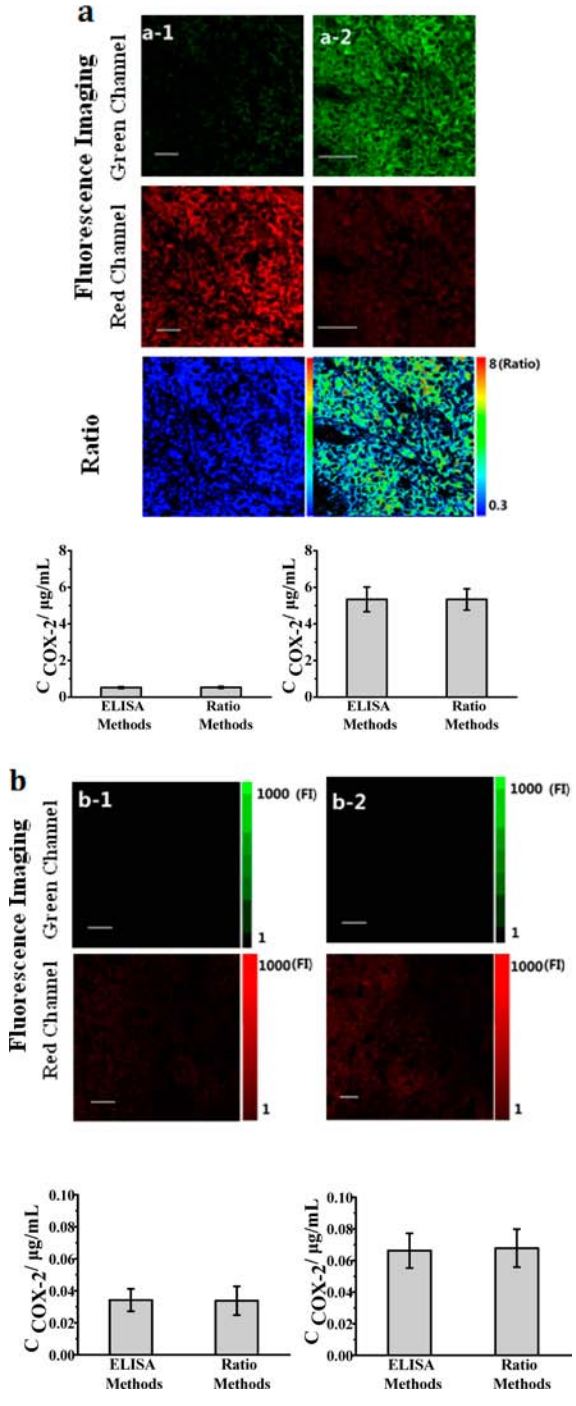

Figure 4. Quantitative detection of COX-2 in live tissues in fluorescence ratio. (a) Quantitative labeling tumor tissues at various stages of development of the tumor by a ratio imaging method. The 5 day and 15 day sarcomas of nude mice were selected as the different stage tumors tissues. (a-1) Sample was the 5 day sarcoma of nude mice. (a-2) Sample was the 15 day sarcoma of nude mice. (b) Quantitative labeling of inflammation tissues at the different stages of inflammation. They are collected in two channels upon excitation at 800 nm with a femtosecond pulse. Condition: NANQ-IMC6 = 30.0 μM; incubation time = 30 min; scale bars = 30 μm.

LB983) was used, all tumors in mice (MDA-MB-231, BEL7402, MKN45) emitted significant fluorescence 30 min after administration of NANQ-IMC6 into the tail vein (Figure 5a and Figure S6). This indicates that the probe had selectively accumulated in tumor lesions. Samples of tumor, inflammation,

dx.doi.org/10.1021/ja4085308 | J. Am. Chem. Soc. 2013, 135, 17469–17475

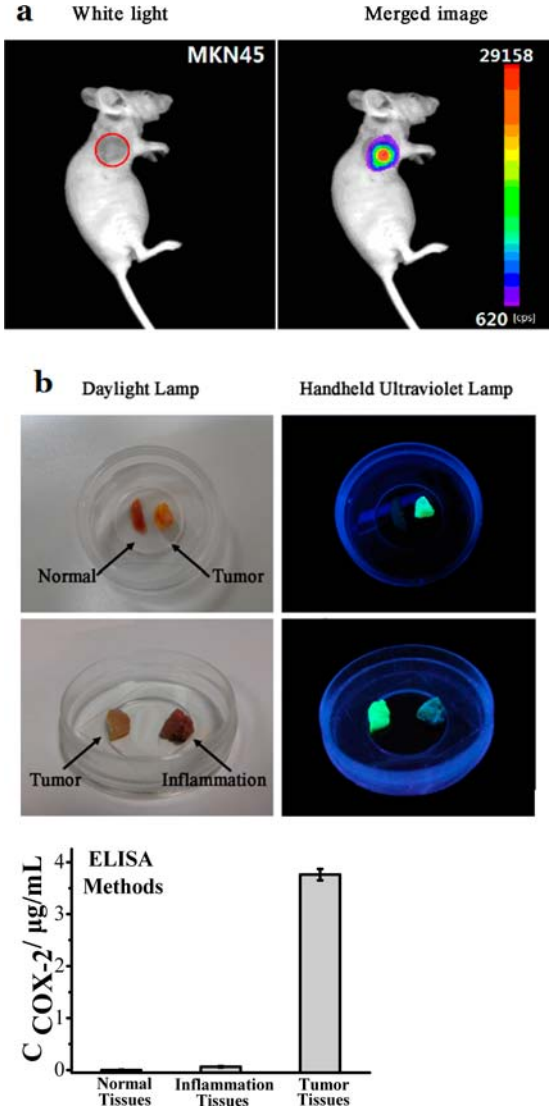

Figure 5. Possibility of naked eye fluorescence-guided resection of tumors. (a) Imaging tumors in vivo. NANQ-IMC6 (30 μM) was injected intravenously (30 μL). The incubation time was 30 min. (b) Visualization of tumor resection by the naked eye under ultraviolet illumination.

and nontumor tissues were obtained from the nude mice with the MDA-MB-231 tumor. When these samples were sprayed with a solution of NANQ-IMC6 in Tris-HCl at pH 8, the tumors could be easily distinguished from both the inflammation and normal tissues by naked eye when illuminated by a hand-held ultraviolet lamp at 365 nm, as demonstrated in Figure 5b.

Rapid Cancer Screening by NANQ-IMC1 with Flow Cytometry. Various cell lines (HeLa, MCF-7, COS-7, and HEK293 cells) were incubated in the probe for 2, 30, or 120 min, and a flow cytometer was used to measure the fluorescence (λ_{ex} = 488 nm, λ_{em} 555 ± 20 nm) in 10 000 individual cells of each population. High-intensity, unimodal signals were obtained for NANQ-IMC1 in each of the two cancer cell lines (HeLa cell and MCF-7), whereas the noncancer cell lines (COS-7 and HEK293) produced very little fluorescence (Figure S7 and Table S2). Low cytotoxicity is another desirable property that allows the probe to be used in general cancer detection. To check that NANQ-IMC1 would not adversely influence cell health, cells were incubated in 8, 16, and 20 μM NANQ-IMC1 solution in complete medium for 4 h, after which cell viability was 97.7, 98.7, and 98.4%, respectively. Moreover, there was little change in the cell count or height of the histograms after longer probe incubation time (120 vs 2 min, Figure S8). The probe is evidently of low toxicity for cancer cell lines, for example, HeLa cell lines.

■ CONCLUDING REMARKS

We exploited the flexibility of the COX-2 substrate-specificity loop by attaching nitro-acenaphthenequinone to indomethacin to form NANQ-IMC6. The fluorescence of NANQ-IMC6 with the form of NANQ-IMC6-folded is quenched in the absence of COX-2. The fluorescence is "turned on" in both inflammations and cancers where COX-2 is overexpressed. Intriguingly, the fluorescent emission is quite different at these two sites with different expression levels of COX-2. In inflammation sites, the fluorescence emission is at 615 nm and increased gradually with increasing COX-2 in the range of 0−0.12 μg/mL. However, in cancer sites, the fluorescence emission at 615 nm decreased gradually, and a new emission at 555 nm showed up and increased with the increasing COX-2 in the range of 0.12−3.32 μg/mL. So, NANQ-IMC6 can not only distinguish normal cells/tissues from cancer cells/tissues but also cleverly distinguish the latter from sites of inflammation using the same methodology. Furthermore, multimodal imaging methods (including one- and two-photon excitation and ratiometric fluorescence), in silico structural analyses, and the outcome of whole-cell assays all demonstrated the rapid and quantitative response of NANQ-IMC6 to COX-2 with high selectivity and sensitivity. Simultaneously, the probe could be used to screen cancer cells by flow cytometry in a rapid, sensitive, and quantitative fashion. To our excitement, spraying with the NANQ-IMC6 solution, cancerous tissue, inflamed tissues, and normal tissues can be accurately discriminated in vivo by the unaided eye using a hand-held ultraviolet lamp emitting at 365 nm. Hence, the probe may have potential application varying from accurate cancer diagnosis to guiding tumor resection during surgery. The former might facilitate various interventional procedures in clinical, such as image-guided biopsy of cancerous tissues, fluorescence-guided laparoscopic surgery of tumors, etc.

■ EXPERIMENTAL SECTION

Synthetic procedures and chemical characterizations of the probes are given in the Supplementary Section. All solvents and reagents used were reagent grade and were used without further purification. Silica gel column chromatography was performed using Sorbent silica gel standard grade, porosity 60 Å, pH range 6.50−7.50. Human cyclooxygenase-2 (COX-2) was purchased from Sigma Chemical Co. (USA). Absorption spectra were measured on a HP-8453 spectrophotometer (Agilent, USA). Fluorescence spectra were obtained with a FP-6500 spectrophotometer (Jasco, Japan). Mass spectral studies were carried out using a LC/Q-Tof mass spectrometer with an autosampler operated in-line with a quantum triple quadrupole instrument in ESI positive or negative ion mode. Mice with tumors (MDA-MB-231, BEL7402, MKN45, S180 sarcoma) were purchased from Slac Laboratory Animal Co. (Shanghai, China).

Quantum Calculations. All the quantum chemical calculations were done with the Gaussian 09 suite.[37] The parameter referred to the work of Han.[38] The geometry optimizations of the dyes were performed using density functional theory (DFT)[39] with Becke's three-parameter hybrid exchange function with Lee−Yang−Parr gradient-corrected correlation functional (B3-LYP functional) and 6-31G **basis set. No constraints to bonds/angles/dihedral angles were

dx.doi.org/10.1021/ja4085308 | J. Am. Chem. Soc. 2013, 135, 17469−17475

applied in the calculations, and all atoms were free to optimize. The electronic transition energies and corresponding oscillator strengths were calculated with time-dependent density functional theory (TD-DFT)[40,41] at the B3LYP/6-31G **level.

Multimodal Quantitative Determination of COX-2 in 100 mM Tris-HCl (pH 8.00). NANQ-IMC6 (5.00 μM) was dissolved in 100 mM Tris-HCl in the presence of COX-2 (0−19.15 μg/mL). Changes in the two-photon fluorescence spectrum as increasing amounts of COX-2 were present were determined using a confocal multiphoton microscope in spectral scanning mode. The tunable filter was automatically stepped in 1 nm increments, from 500 to 750 nm. The excitation wavelength was 800 nm with a mode-locked titanium:sapphire laser source (Coherent Chameleon, 90 MHz, 200 fs), and output power was 1230 mW, which corresponded to approximately 10 mW average power in the focal plane. Two-photon fluorescence spectra were sequentially captured at each wavelength interval. The fluorescence ratio spectra were obtained by the ratio of fluorescence intensity (I_{555}/I_{615}) with the amount of COX-2.

Cell Culture and Staining with NANQ-IMC6. Cell lines were purchased from the Chinese Academy of Science Cell Library (Shanghai, China). Cells were cultured for 3 days in phenol-red-free Dulbecco's modified Eagle's medium (DMEM, WelGene) supplemented with penicillin/streptomycin and 10% fetal bovine serum (Gibco) in a 5% CO_2 incubator at 37 °C. One day before imaging, cells were seeded into a glass-bottomed dish (MatTek, 35 mm dish with 20 mm well). The next day, the cells were incubated with NANQ-IMC6 and then washed with phosphate buffered saline three times.

Inflammation, Tumor, and Normal Tissue Slice Culture and Staining with NANQ-IMC6. Carrageenan (50 μL 1% in sterile saline) was injected in the rear left footpad of C57BL/6 mice, and the mice were bred for 5 and 15 days. Then, the inflammation tissue slices were prepared from the relevant mice. Tumor tissue slices were prepared from nude mice with S180 sarcoma. Normal tissue slices were prepared from livers of nude mice. The slices were cut at 700 μm using a vibrating-blade microtome in artificial cerebrospinal fluid (ACSF; 124 mM NaCl, 3 mM KCl, 26 mM $NaHCO_3$, 1.25 mM NaH_2PO_4, 10 mM D-glucose, 2.4 mM $CaCl_2$, and 1.3 mM $MgSO_4$). Slices were incubated with NANQ-IMC6 (30 μM) in ACSF bubbled with 95% O_2 and 5% CO_2 for 30 min at 37 °C and then washed three times with ACSF and transferred to a glass-bottomed dish (MatTek, 35 mm dish with 20 mm well).

Fluorescence Imaging in the Cells and Tissues. Two-photon fluorescence imaging of NANQ-IMC6 in cells and tissues were obtained with a spectral confocal multiphoton microscope (Olympus, FV1000) with a high-performance mode-locked titanium:sapphire laser source (MaiTai, Spectra-Physice, USA). Numerical aperture was 1.42 (oil) and 1.30 (sil). The excitation wavelength was 800 nm, and output power was 1230 mW, which corresponded to approximately 10 mW average power in the focal plane. Images were collected in two channels (green channel = 535−565 nm, red channel = 590−620 nm). To obtain two-photon images, internal PMTs were used to collect the signals in an 8 bit unsigned 1024 × 1024 pixels. The ratio images of the green channel and red channel were analyzed by the Image-Pro Express 6.3 software.

Tumor Model in Mice. All procedures were carried out in compliance with the Guide for the Care and Use of Laboratory Animal Resources and the National Research Council and were approved by the Institutional Animal Care and Use Committee of the NIH. Three human cancer cell lines were used for in vivo studies: MDA-MB-231, BEL7402, and MKN45. The tumor implants were established by subskin injection of 1×10^6 to 2×10^6 cells suspended in 200−300 μL of PBS in nude mice. Each cell line required different duration of time to produce multiple disseminated tumors of about 0.5 cm in size. Experiments with tumor-bearing mice were performed about 20 days, when implants grew to about 1 mm in size.

Fluorescence Imaging in Mice. The mice with tumors were given a tail vein injection of NANQ-IMC6 (30 μL of 30 μM). After being injected with NANQ-IMC6 for 30 min, the mice were imaged using a NightOWL II LB983 small animal in vivo imaging system with a 488 nm excitation laser and a 550 ± 10 nm emission filter.

Enzyme-Linked Immunosorbent Assay (ELISA) To Determine the Amount of COX-2. This assay used the ABC double-antibody sandwich ELISA method. A cyclooxygenase-2 kit (human, double-antibody method, 96t) was purchased from Sigma Chemical Co. (USA). Cells and tissues were homogenized and stored at 2−8 °C. This part of the work was completed commercially by Dalian Medical University. The ELISA assay experiment was carried out according to literature procedures[19] and manufacturer's instructions of COX-2.

Flow Cytometry. Cells (1×10^5) from each cell line were plated into a six-chamber culture well and incubated for 16 h. NANQ-IMC6 was added to the culture medium, and the cells were incubated for 30 min. A 488 nm argon ion laser was used for excitation. Signals from cells were collected with a 555 nm band-pass filter. Cells were analyzed in a FAC scan cytometer (Becton Dickinson), and all data were analyzed with Cell Quest software.

■ ASSOCIATED CONTENT

Supporting Information

Synthetic protocol and characterization data for NANQ-IMC6; quantitative detection of COX-2 in vitro; photophysical properties of NANQ-IMC6; evaluation of the two-photon performance of NANQ-IMC6; imaging tumors in vivo; screening for cancer cells by flow cytometry; assessing the cytotoxicity of NANQ-IMC6. This material is available free of charge via the Internet at http://pubs.acs.org.

■ AUTHOR INFORMATION

Corresponding Author

fanjl@dlut.edu.cn; pengxj@dlut.edu.cn

Notes

The authors declare no competing financial interest.

■ ACKNOWLEDGMENTS

This work was financially supported by NSF of China (21136002, 20923006, 21376039, and 21076032), National Basic Research Program of China (2013CB733702), and Ministry of Education (NCET-12-0080). Hanyu Yang, Fan An, and Mingxi Yu are thanked for the assistance in the provision of biological samples, and Dr. Zhaokui Wan and Dr. Erik Hetts are acknowledged for careful reviewing of the manuscript and constructive comments.

■ REFERENCES

(1) Greenlee, R. T.; Murray, T.; Bolden, S.; Wingo, P. A. *Ca-Cancer J. Clin.* **2000**, *50*, 7−33.
(2) Urano, Y.; Sakabe, M.; Kosaka, N.; Ogawa, M.; Mitsunaga, M.; Asanuma, D.; Kamiya, M.; Young, M. R.; Nagano, T.; Choyke, P. L. *Sci. Transl. Med.* **2011**, *3*, 110−119.
(3) Denkert, C.; Winzer, K. J.; Müller, B. M.; Weichert, W.; Pest, S.; Köbel, M.; Kristiansen, G.; Reles, A.; Siegert, A.; Guski, H.; Hauptmann, S. *Cancer* **2003**, *97*, 2978−2987.
(4) Toyokuni, T.; Kumar, J. S.; Walsh, J. C.; Shapiro, A.; Talley, J. J.; Phelps, M. E.; Herschman, H. R.; Barrio, J. R.; Satyamurthy, N. *Bioorg. Med. Chem. Lett.* **2005**, *15*, 4699−4702.
(5) de Vries, E. F.; Doorduin, J.; Dierckx, R. A.; van Waarde, A. *Nucl. Med. Biol.* **2008**, *35*, 35−42.
(6) Fass, L. *Mol. Oncol.* **2008**, *2*, 115−52.
(7) Frangioni, J. V. *J. Clin. Oncol.* **2008**, *26*, 4012−4021.
(8) Weissleder, R.; Pittet, M. J. *Nature* **2008**, *452*, 580−589.
(9) Sung, Y. K.; Hwang, S. Y.; Kim, J. O.; Bae, H. I.; Kim, J. C.; Kim, M. K. *Mol. Cells* **2004**, *17*, 35−38.
(10) Mrena, J.; Wiksten, J. P.; Kokkola, A.; Nordling, S.; Ristimäki, A.; Haglund, C. *Tumour Biol.* **2010**, *31*, 1−7.
(11) Tucker, O. N.; Dannenberg, A. J.; Yang, E. K.; Zhang, F.; Teng, L.; Daly, J. M.; Soslow, R. A.; Masferrer, J. L.; Woerner, B. M.; Koki, A. T.; Fahey, T. J. *Cancer Res.* **1999**, *59*, 987−990.

(12) Eberhart, C. E.; Coffey, R. J.; Radhika, A.; Giardiello, F. M.; Ferrenbach, S.; Dubois, R. N. *Gastroenterology* **1994**, *107*, 1183−1188.
(13) Otto, J. C.; Smith, W. L. *J. Lipid Mediators Cell Signalling* **1995**, *12*, 139−156.
(14) Kam, P. C.; See, A. U. *Anaesthesia* **2000**, *55*, 442−449.
(15) Simmons, D. L.; Botting, R. M.; Hla, T. *Pharmacol. Rev.* **2004**, *56*, 387−437.
(16) Katori, M.; Majima, M. *Inflamm. Res.* **2000**, *49*, 367−392.
(17) Nantel, F.; Nantel, F.; Denis, D.; Gordon, R.; Northey, A.; Cirino, M.; Metters, K. M.; Chan, C. C. *J. Pharmacol.* **1999**, *128*, 853−859.
(18) Crofford, L. J. *J. Rheumatol.* **1997**, *49*, 15−19.
(19) Samad, T. A.; Moore, K. A.; Sapirstein, A.; Billet, S.; Allchorne, A.; Poole, S.; Bonventre, J. V.; Woolf, C. J. *Nature* **2001**, *410*, 471−475.
(20) Subbaramaiah, K.; Dannenberg, A. J. *Trends Pharmacol. Sci.* **2003**, *24*, 96−102.
(21) Kandil, H. M.; Tanner, G.; Smalley, W.; Halter, S.; Radhika, A.; Dubois, R. N. *Dig. Dis. Sci.* **2001**, *46*, 785−789.
(22) Rizzo, M. T. *Clin. Chim. Acta* **2011**, *412*, 671−687.
(23) Uddin, M. J.; Crews, B. C.; Blobaum, A. L.; Kingsley, P. J.; Gorden, D. L.; McIntyre, J. O.; Matrisian, L. M.; Subbaramaiah, K.; Dannenberg, A. J.; Piston, D. W.; Marnett, L. J. *Cancer Res.* **2010**, *70*, 3618−3627.
(24) Zhang, H.; Fan, J. L.; Wang, J. Y.; Zhang, S. Z.; Dou, B. R.; Peng, X. J. *J. Am. Chem. Soc.* **2013**, *135*, 11663−11669.
(25) Kurumbail, R. G.; Stevens, A. M.; Gierse, J. K.; McDonald, J. J.; Stegeman, R. A.; Pak, J. Y.; Gildehaus, D.; Miyashiro, J. M.; Penning, T. D.; Seibert, K.; Isakson, P. C.; Stallings, W. C. *Nature* **1996**, *384*, 644−648.
(26) Upadhyay, A. K.; Horton, J. R.; Zhang, X.; Cheng, X. *Curr. Opin. Struct. Biol.* **2011**, *21*, 750−760.
(27) Khan, A. A.; Iadarola, M.; Yang, H. Y.; Dionne, R. A. *J. Pain* **2007**, *4*, 349−354.
(28) Picot, D.; Loll, P. J.; Garavito, R. M. *Nature* **1994**, *367*, 243−249.
(29) Luong, C. *Nat. Struct. Biol.* **1996**, *3*, 927−933.
(30) Bhattacharyya, D. K.; Lecomte, M.; Rieke, C. J.; Garavito, R. M.; Smith, W. L. *J. Biol. Chem.* **1996**, *271*, 2179−2184.
(31) Kalgutkar, A. S.; Crews, B. C.; Rowlinson, S. W.; Marnett, A. B.; Kozak, K. R.; Remmel, R. P.; Marnett, L. J. *Proc. Natl. Acad. Sci. U.S.A.* **2000**, *97*, 925−930.
(32) Terpetschnig, E.; Szmacinski, H.; Ozinskas, A.; Lakowicz, J. R. *Anal. Biochem.* **1994**, *217*, 197−204.
(33) Jisha, V. S.; Arun, K. T.; Hariharan, M.; Ramaiah, D. *J. Am. Chem. Soc.* **2006**, *128*, 6024−6025.
(34) Abugo, O. O.; Nair, R.; Lakowicz, J. R. *Anal. Biochem.* **2000**, *279*, 142−150.
(35) Furuta, T.; Wang, S. S.; Dantzker, J. L.; Dore, T. M.; Bybee, W. J.; Callaway, E. M.; Denk, W.; Tsien, R. Y. *Proc. Natl. Acad. Sci. U.S.A.* **1999**, *96*, 1193−1200.
(36) Andreev, O. A.; Dupuy, A. D.; Segala, M.; Sandugu, S.; Serra, D. A.; Chichester, C. O.; Engelman, D. M.; Reshetnyak, Y. K. *Proc. Natl. Acad. Sci. U.S.A.* **2007**, *104*, 7893−7898.
(37) Frisch, M. J.; Trucks, G. W.; Schlegel, H. B.; Scuseria, G. E.; Robb, M. A.; Cheeseman, J. R.; Scalmani, G.; Barone, V.; Mennucci, B.; Petersson, G. A.; Nakatsuji, H.; Caricato, M.; Li, X.; Hratchian, H. P.; Izmaylov, A. F.; Bloino, J.; Zheng, G.; Sonnenberg, J. L.; Hada, M.; Ehara, M.; Toyota, K.; Fukuda, R.; Hasegawa, J.; Ishida, M.; Nakajima, T.; Honda, Y.; Kitao, O.; Nakai, H.; Vreven, T.; Montgomery, J. A., Jr.; Peralta, J. E.; Ogliaro, F.; Bearpark, M.; Heyd, J. J.; Brothers, E.; Kudin, K. N.; Staroverov, V. N.; Kobayashi, R.; Normand, J.; Raghavachari, K.; Rendell, A.; Burant, J. C.; Iyengar, S. S.; Tomasi, J.; Cossi, M.; Rega, N.; Millam, J. M.; Klene, M.; Knox, J. E.; Cross, J. B.; Bakken, V.; Adamo, C.; Jaramillo, J.; Gomperts, R.; Stratmann, R. E.; Yazyev, O.; Austin, A. J.; Cammi, R.; Pomelli, C.; Ochterski, J. W.; Martin, R. L.; Morokuma, K.; Zakrzewski, V. G.; Voth, G. A.; Salvador, P.; Dannenberg, J. J.; Dapprich, S.; Daniels, A. D.; Farkas, O.; Foresman, B.; Ortiz, J. V.; Cioslowski, J.; Fox, D. J. *Gaussian 09*, revision A.02; Gaussian, Inc.: Wallingford, CT, 2009.
(38) Zhou, L. C.; Zhao, G. J.; Liu, J. F.; Han, K. L.; Wu, Y. K.; Peng, X. J.; Sun, M. T. *J. Photochem. Photobiol. A* **2007**, *187*, 305−310.
(39) Dreizler, M. R.; Gross, E. K. U. *Density Functional Theory*; Springer-Verlag: Heidelberg, Germany, 1990.
(40) Gross, E. K. U.; Kohn, W. *Phys. Rev. Lett.* **1985**, *55*, 2850−2852.
(41) Stratmann, R. E.; Scuseria, G. E.; Frisch, M. J. *J. Chem. Phys.* **1998**, *109*, 8218−8224.